

High resolution phase gradient mapping as a tool for the detection and analysis of local field disturbances

H. de Leeuw¹, P. R. Seevinck¹, G. H. van de Maat¹, and C. J. Bakker¹

¹Image Sciences Institute, University Medical Center Utrecht, Utrecht, Netherlands

Introduction Since the early days of MRI phase mapping has been used to study object induced perturbations of the phase of the MR signal. Usually these phase perturbations result in signal loss due to signal dephasing. In the context of the detection of, for example, paramagnetic or diamagnetic contrast agents there is much interest in selectively turning this dark contrast into a positive contrast, as well as in quantifying the susceptibility effect. Special sequences have been developed to selectively obtain positive contrast [1, 2]. These sequences, however, in general need information on the local field to achieve the desired positive contrast [1, 2]. In previous work of other groups the echo shift phenomenon was used to obtain positive contrast on local field distortions, without the need of a special sequence or prior knowledge [3]. Disadvantages of this technique include a reduction of the resolution and absence of error measures, other than obtained values for the contrast to noise. The technique presented in this abstract does not use the echo shift artifact, but the signal itself to determine the phase gradient [4]. The proposed technique does not need phase unwrapping, maintains resolution and provides simple error measures. Experimental validation of the method is done with a coaxial cylinder phantom with a known susceptibility distribution. We further show the applicability of the technique in depicting and analyzing the distribution of holmium-loaded microspheres [5] in an ex-vivo rabbit liver.

Materials & Methods The phase derivative was determined from the real and imaginary parts of the spin density (ρ) and the derivative of the spin density ($\partial\rho/\partial s$) [6]:

$$\frac{\partial\varphi}{\partial s} = \frac{\partial}{\partial s} \arctan\left[\frac{I}{R}\right] = \left(R\frac{\partial I}{\partial s} - I\frac{\partial R}{\partial s}\right)(R^2 + I^2)^{-1} = \left(R\text{Im}\left[\frac{\partial\rho}{\partial s}\right] - I\text{Re}\left[\frac{\partial\rho}{\partial s}\right]\right)(R^2 + I^2)^{-1} \quad (1)$$

where s denotes the direction of the derivative. The derivative of the spin density was obtained by applying the Fourier derivative theorem [6], which corresponds to multiplying the complex data in the Fourier domain by $2\pi i k_s$, with k_s the coordinate in the Fourier domain, corresponding to s . By considering an MR acquisition, this method is shown to provide the best derivative of the spin density one can obtain.

Any MR acquisition consists of a spin density (ρ), measured in an area of interest (FOV) with a certain resolution. These measurement operations, as well as the derivative operation, are described by convolutions. This allows us to rewrite the spin density derivative by using the associativity principle and the Fourier derivative theorem [6]:

$$\begin{aligned} \frac{\partial}{\partial s} \rho_{\text{measured}}(\vec{x}) &= \rho(\vec{x}) * U(\vec{x}) * S(\vec{x}) * D_s(\vec{x}) = \rho(\vec{x}) * D_s(\vec{x}) * U(\vec{x}) * S(\vec{x}) \\ &= F^{-1}\left[\rho(k) \cdot 2\pi i k_s\right] * U(\vec{x}) * S(\vec{x}) = \frac{\partial\rho}{\partial s}(\vec{x}) * U(\vec{x}) * S(\vec{x}) \end{aligned} \quad (2)$$

where $*$ denotes a convolution, $D_s(x)$ the derivative operator, $U(x)$ the truncation function (FOV), $S(x)$ the sampling function (resolution) and F^{-1} the inverse Fourier transform. Equation 2 shows that, if the phase derivative is determined in this way, it is exactly as good as the acquisition allows. There is no loss of resolution and no phase unwrapping is needed. Equation 1 further implies that the error in the phase derivative is approximately $\sqrt{2}$ times the SNR in the magnitude.

3D gradient echo imaging was performed on a 3.0-T clinical whole body system (Achieva 3.0T, Philips Medical Systems, Best, The Netherlands) using a quadrature head coil. Scan parameters included: TE=3.8ms, TR=8.2 ms, $\theta=10^\circ$, FOV: $128 \times 128 \times 128$ mm³, matrix: $128 \times 128 \times 128$ and NEX=3. Experiments were done with a coaxial cylinder phantom with a known susceptibility difference between inner and outer cylinder ($\Delta\chi = -10.3$ ppm) and an ex-vivo rabbit liver. Holmium-loaded microspheres [5] were administered through a catheter in the portal vein of the liver. In total 40mg (4x10) microspheres were injected into the liver. The phase derivative was set to zero for SNR in the magnitude below three. The phase derivative magnitude was calculated by taking the square root of the sum of squares of the vectorial components. For the liver, phase derivative magnitude maps were averaged using a Gaussian filter (kernel size 3, width 1 pixel). For evaluation purposes six central slices were summed and windowed (0 to 0.4 rad mm⁻¹ for 0 mg, 0.4 to 6π rad mm⁻¹ otherwise).

Results Figure 1 shows a phase image of the phantom (a) and the corresponding phase derivative images along the x-direction (b) and the z-direction (B_0) (c). The phase derivative images are easier to interpret, while keeping all information of the phase images. The profile of the $\nabla_z\varphi$, from top to bottom along z , through the cylinder center is shown in figure 2. The black line represents the theoretical profile (infinite cylinder model, since $\nabla_y\varphi = 0$ [3, 4, 6]), while the circles show the calculated derivative with error margin. Nearly perfect quantitative agreement is obtained. Close to the inner cylinder intravoxel dephasing and undersampling result in poor correspondence. Figure 3 shows magnitude images (top, a-c) and phase derivative magnitude images (bottom, d-f) of the rabbit liver with 0 (a, d), 20 (b, e) and 40 mg (c, f) microspheres injected. The intense spot in the center of the images (black for the magnitude and white for the phase derivative magnitude) is due the inserted catheter. The window-level of the phase derivative magnitude images allows highlighting the (physically) most relevant structures. In the magnitude images, for example, all four liver lobes and some irregular flow of the fluid around the liver can be discerned. Figure 3d shows the edges of the lobes, along with some vasculature and flow effects. In figure 3e and 3f these background effects are suppressed by using the maximum of the window in figure 3d as minimum in figure 3e and 3f. In the magnitude images the holmium results in dark vesicles; in the phase derivative magnitude positive contrast is created. For increasing amounts of microspheres, the gradient strength increases, resulting in stronger positive contrast (figure 3e and 3f). No microspheres are found in the right lobe, since it keeps its intensity in the magnitude images and is suppressed in figure 3e and 3f. Some clustering of microspheres can be observed in both the magnitude image (black spots) and the phase derivative magnitude images (white spots).

Conclusion We have demonstrated a post processing technique -phase gradient mapping- that enables us to generate positive contrast of magnetically labeled substances. It furthermore can be used as a tool for the detection and analysis of local field inhomogeneities. The technique can be applied without loss of resolution, does not need phase unwrapping and allows simple error estimations. Phase gradient mapping provides quantitative values and may be expected to find application in many areas, e.g., in studies concerned with the quantification or characterization of field distortions due to contrast agents [1, 3, 4].

References [1] C.J.G. Bakker et al. *MRM* 2006;55:92-97 [2] M. Stuber et al. *MRM* 2007;58:1072-1077 [3] H. Dahnke et al. *MRM* 2008;60:595-603 [4] C.J.G. Bakker et al. *PMB* 2008(18);53:N349-N358 [5] J.F. Nijssen et al. *Radiology* 2004(2);231:491-499 [6] Haacke et al. *Magnetic Resonance Imaging*, Wiley-Liss 1999

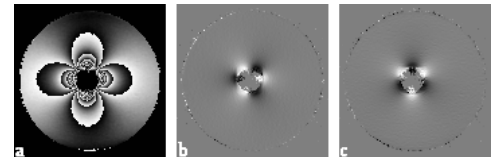


Figure 1: Phase (a) and phase derivatives $\nabla_x\varphi$ (b), $\nabla_z\varphi$ (c) of the coaxial cylinder phantom.

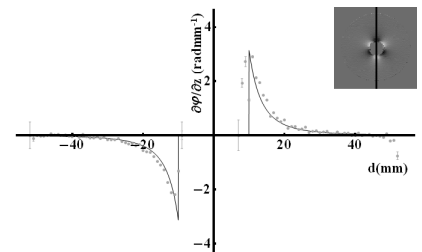


Figure 2: Theoretical (line) and experimental phase gradient ($\nabla_z\varphi$, dots) through the center of the coaxial cylinder phantom.

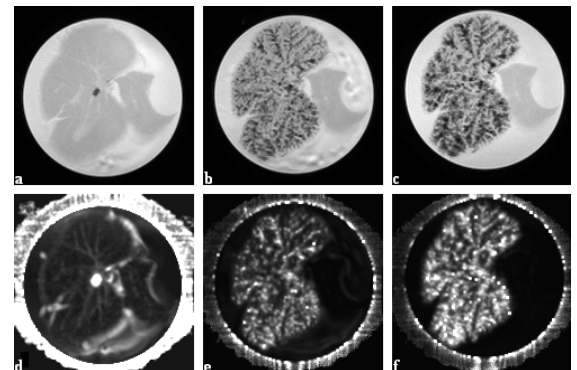


Figure 3: Magnitude (top) and phase derivative magnitude ($|\nabla\varphi|$, bottom) images of a rabbit liver after injection of, from left to right, 0, 20 and 40 mg microspheres.